*Tellus (1994), 46A, 34–51*
*Printed in Belgium – all rights reserved*


**TELLUS**
*ISSN 0280–6495*

# Water vapor transport in the NCAR CCM2

By DAVID L. WILLIAMSON* and PHILIP J. RASCH, *National Center for Atmospheric Research***, *P.O. Box 3000, Boulder, Colorado 80307-3000, USA*

(Manuscript received 16 December 1992; in final form 5 July 1993)

ABSTRACT

The NCAR Community Climate Model, Version 2, uses the spectral transform method for the underlying dry dynamical fluid flow component, and a monotonic, semi-Lagrangian transport algorithm for water vapor specific humidity. The reasons for this choice of 2 different approaches for these different components are reviewed, and the details of the implementation of the transport algorithm are presented. The properties of the transport scheme are described in the context of a 20-year control simulation. This simulation is also compared to one using the spectral transform method for water vapor transport. Neither numerical approach is perfect. The semi-Lagrangian method requires arbitrary corrections to conserve mass, and the spectral method requires the filling of nonphysical negative values of specific humidity. The analysis shows that the balance of processes that produces the climate of CCM2 is very sensitive to the discrete water vapor transport algorithm. The spectral transport method clearly has shortcomings. The negative filler is a dominant process in significant regions and leads to an incorrect balance of the moisture budget. The mass conservation adjustment of the semi-Lagrangian method seems to be cosmetic and has no identified adverse effect on the simulation.

## 1. Introduction

Water vapor plays a fundamental rôle in many atmospheric processes, the combination of which produces the delicate balance yielding a climate equilibrium. It provides a direct transfer of energy between components of the climate system such as land, sea-ice, ocean, and atmosphere. It is the primary greenhouse gas in the atmosphere providing a strong influence on the radiative balance of the overall system and, in particular, on the radiative heating of the atmosphere. The clouds that form when it is transformed to liquid or ice phase strongly modulate the radiative heating. There is no hope in modeling the climate of the atmosphere correctly if water vapor is not well-modeled.

Despite the crucial importance of water vapor in the climate system, it has often been poorly treated in three-dimensional atmospheric climate models. Schemes developed, and which are ideal for modeling large, global scale dynamical motions have simply been adapted to water vapor almost as an afterthought, without concern for whether they actually provide a satisfactory basis of approximation. The popular spectral transform method provides an example of such an application. The spectral transform method is an extremely good method for approximating large scale, global atmospheric dynamical motion, hence its well deserved popularity. The fields involved (wind, temperature, and pressure) are relatively smoothly varying, or seem to be, when small scale features, such as fronts, are smoothed to be consistent with the scales retained in the underlying discrete representation. This implicit smoothing does not seem to be detrimental to the simulation of the larger scale features.

Water vapor, on the other hand, is poorly treated by the spectral transform method. Its characteristics are vastly different from those of

* Corresponding author.
** The National Center for Atmospheric Research is sponsored by the National Science Foundation.

mass and momentum. Water vapor varies by several orders of magnitude between the equator and poles and between the earth's surface and the hygropause in the lower stratosphere. It has strong gradients with small scale structures and is continually forced on the smallest scales by the subgrid scale process components of the models. Smoothing these gradients and small scale structures in the water vapor field does seem to be detrimental to the physical processes included in these models. This is, in part, because relative, rather than absolute, changes in water vapor (over its entire range of variation) are important in many of the physical processes being modeled. The problems associated with the spectral treatment of water vapor are now well known. Undershooting leads to negative values, which are particularly noticeable in the polar regions (Laprise, 1988), but also occur in the tropical troposphere (Rasch and Williamson, 1990b). Overshooting leads to spurious modulation of regions of light precipitation (Williamson, 1990), which can lead to spurious clouds. Because spectral methods attempt to minimize the error, in an absolute sense, over the entire (horizontal) domain, the relative error is extremely large where the field is small, and this has a very detrimental effect on many processes. Ad hoc procedures to deal with unphysical negative values, such as filling algorithms, are significant components in the water vapor forecast (Rasch and Williamson, 1991), not cosmetic corrections with insignificant interaction with the physical components of the model. Ostiguy and Laprise (1990) have studied, in a more fundamental way, the side effects of various remedies that have been applied to negative regions. No procedures have been proposed that attempt to mollify the effect of water vapor overshooting on the physical parameterizations.

Because of the shortcomings of the spectral transform method for water vapor transport, but suitability of the method for global dynamical models, we earlier proposed to combine shape-preserving semi-Lagrangian transport of water vapor (and any additional desired constituents) with global spectral transform models (Rasch and Williamson, 1990b; 1991). The semi-Lagrangian method was chosen because it offers a natural application to a global domain and spherical geometry. There are many very attractive modern numerical transport schemes for applications in Cartesian geometry (Rood, 1987), but most of these do not yet have economical variants for the global domain. A review of the difficulties involved in modeling global transport and of various general approaches, but not of the details of modern schemes themselves, is provided by Williamson (1992). Shape preservation, which provides a nonlinear constraint on the scheme, was introduced to allow the scheme to be able to accept and maintain sharp gradients without admitting over and under shooting (Rasch and Williamson, 1990a; Williamson and Rasch, 1989.) The ability of this numerical advection scheme to transport discontinuous atmospheric constituents is illustrated in Boville et al. (1991). The success of the combined approach in an atmospheric general circulation model is demonstrated in Rasch and Williamson (1991) and in a numerical weather prediction model in Williamson (1990).

The members of the Climate Modeling Section at NCAR have recently completed the development of a new version of the Community Climate Model, CCM2. This model uses the spectral transform method for the dry dynamical aspects, and the shape preserving, semi-Lagrangian transport algorithm for water vapor. It also has provision for an arbitrary number of additional transported variables such as cloud water or chemical constituents for research applications and future development. Horizontal diffusion is not applied to water vapor or the additional transported variables. In this paper, we provide details (in an Appendix) of the constituent transport scheme as implemented in CCM2. Essentially, the semi-Lagrangian method is based on trajectories which end at time $t+\Delta t$ at the grid points at which the forecast is desired. In our case, those points comprise the Gaussian grid adopted by the spectral transform method. Values of quantities undergoing only advection are preserved along the trajectories. Thus, values at the beginning of the trajectories at time $t-\Delta t$ provide the desired forecast values at the ends at $t+\Delta t$. Since the beginning of the trajectories does not necessarily coincide with grid points, the values are obtained there by interpolation. We chose monotone interpolation, as mentioned above. Physical processes, such as condensation, convection, and mixing in the planetary boundary layer, are handled in a time split manner to isolate the advective component. Details are provided in the appendix.

In this paper, we also describe the properties of the transport scheme in the control simulation with CCM2 and contrast them to those of the spectral transform method. In addition, we compare the sensitivity of CCM2 simulations to these two water vapor transport methods with the sensitivity of the earlier CCM1 simulations. The new CCM2 is very different from the earlier CCM1; it has modern physical parameterizations, higher vertical and horizontal resolution, and the suite of physical parameterizations is tuned with the semi-Lagrangian water vapor transport scheme in place, rather than the spectral transform scheme.

## 2. Brief description of CCM2

Almost all aspects of CCM2 offer improvements over CCM1. These include both resolved dynamics and physical parameterizations. The only unchanged aspects are the semi-implicit, leap frog time integration scheme, the spectral transform method for dry dynamics, and the fourth order horizontal diffusion applied to the dynamical variables. These aspects are documented in Williamson et al. (1987). The CCM2 adopts a hybrid vertical coordinate, ($\eta$), which is terrain-following near the surface (traditional sigma) and becomes a pressure coordinate above about 100 mb (Simmons and Burridge, 1981 and Simmons and Strüfing, 1981, 1983). The vertical finite difference approximations collapse to those of CCM1 when the hybrid coordinate is set to be sigma. The standard configuration for CCM2 is T42 spectral resolution with an accompanying 128 longitude by 64 latitude point Gaussian grid and 18 vertical levels with an explicit lid at 3 mb. It uses a 20 minute time step by dynamically adjusting the spectral resolution of the top layer to maintain a Courant number of less than one. More details of the numerical/dynamical aspects are provided in Hack et al. (1993).

All the physical parameterizations of CCM1, except the large scale stable rain, have been replaced or augmented for CCM2. The planetary boundary layer (pbl) parameterization is a nonlocal scheme based on the work of Troen and Mahrt (1986) and Holtslag et al. (1990). The boundary layer depth is calculated explicitly. In the boundary layer, nonlocal eddy diffusivity and counter gradient transport terms are applied. Details of the implementation in CCM2 and a comparison of its performance with the local eddy diffusivity of CCM1 are given in Holtslag and Boville (1993). Above the pbl, the local vertical diffusion scheme of CCM1 is retained, although the functional dependence of the diffusion coefficients is somewhat different. McFarlane's (1987) parameterization of momentum flux divergence by stationary gravity waves is included.

A simple mass flux scheme developed by Hack (1993) is used to represent all types of moist convection. This scheme is based on a three level conceptual model, with convergence and entrainment in the first level, condensation and rain out in the middle level, and limited detrainment in the top level. The convective model is applied to three contiguous CCM levels, starting from the bottom of the model and shifting up successively, one level at a time, after which the column is stable. The convection parameterization makes use of temperature and moisture perturbations from the pbl parameterization to determine the thermodynamic properties of ascending parcels. Hack (1993) compares the performance of this scheme with that of moist convective adjustment of CCM1. CCM2 contains new cloud fraction and cloud albedo parameterizations. The cloud fraction parameterization is a generalization of Slingo's (1987) and depends on relative humidity, vertical motion, static stability, and convective precipitation rate. Clouds are permitted at all tropospheric model levels except the lowest. The cloud emissivities are determined from the liquid water path. The cloud liquid water path is determined by integrating through the appropriate section of a specified vertical liquid water concentration profile, which is a function of latitude.

The solar radiative heating is computed using a delta-Eddington parameterization with 18 spectral bands (Briegleb, 1992). Both diurnal and annual cycles are included. A Voigt correction has been incorporated in the longwave parameterization (Kiehl and Briegleb, 1991). Radiative heating rates are calculated every hour and absorptivities/emissivities are calculated every 12 h. The land temperature is calculated with soil heat capacity represented by a 4-layer diffusion model, with heat capacities specified for each layer to capture the major observed climatological cycles. The land has specified soil hydrologic properties. Sea surface

temperatures are specified by linear interpolation between the climatological monthly mean values of Shea et al. (1990). Surface fluxes are calculated with stability-dependent transfer coefficients between the surface and first model level. They are also modified from those in CCM1 and detailed in Holtslag and Boville (1993).

## 3. Simulation description

The control simulation consists of a 20-year integration of CCM2. This simulation started from 1 September of a previous shorter simulation with CCM2 and represents a state from the model climate. There is no additional drift toward model climate in the twenty year control, and the entire period can be safely used for analysis. This simulation will be referred to as the control or semi-Lagrangian version. However, it should be kept in mind that only the water vapor is treated with the semi-Lagrangian method.

The experimental version was run for one year starting 1 September of the eleventh year of the control run. It used the spectral transform method for horizontal water vapor transport and finite differences for the vertical transport. These are the same approximations as used for advection in the dry dynamics. This version will be referred to as the spectral simulation, although it should be kept in mind that the vertical advection actually used finite difference approximations. Although this simulation was begun 1 September, first order effects, due to tropospheric water vapor, should be seen in the January average as the tropospheric water vapor is replaced on a 30-day time scale. Second order effects due to stratospheric water vapor may not be felt in January since the water vapor processes are much slower there.

## 4. Global averages

We first consider the global average values of the computational terms added to the two models to compensate for flaws in the numerical approximations. We refer to these terms as fixers. The semi-Lagrangian method is not a priori conservative, and we observe in practice that it does not conserve to the degree desired. Therefore, we have introduced a variational procedure to restore the global average moisture every time step after advection (Rasch and Williamson, 1990b). This procedure is described in detail in the Appendix. The method modifies the moisture field in proportion to the specific humidity and in proportion to the change made by the advection. Therefore the correction is smallest where the specific humidity is small and where the advective tendency is small. The effect on the simulation of not including this conservation correction is discussed in Section 7, after the semi-Lagrangian and spectral simulations are compared.

The spectral method does not a priori conserve water vapor either, but here we observe that, in practice, it does conserve extremely well, and no correction is required for conservation. On the other hand, as mentioned above, it produces negative values that must be brought at least to zero before proceeding with the calculations. Therefore, the model includes a negative borrower or filler, as described in Williamson et al. (1987). This scheme first attempts to borrow from the immediate height-longitude neighbors. If sufficient moisture is not available locally, it then simply eliminates the negative values and removes moisture proportionally from all points. The global average values of these fixers are listed in Table 1, along with the averages of precipitable water and the precipitation components for com-

Table 1. *Global average values of various quantities associated with water vapor from semi-lagrangian and spectral simulations*

| | January | | July | |
|---|---|---|---|---|
| | semi-lagrangian | spectral | semi-lagrangian | spectral |
| precipitable water (mm) | 23.60 | 23.09 | 28.42 | 28.10 |
| convective precip (mm/day) | 2.63 | 2.59 | 3.03 | 3.00 |
| stable precip (mm/day) | 0.85 | 0.95 | 0.77 | 0.87 |
| total precip (mm/day) | 3.48 | 3.54 | 3.81 | 3.87 |
| fixer (mm/day) | −0.10 | 0.32 | −0.08 | 0.25 |

parison. The semi-Lagrangian fixer is the amount that is added to ensure conservation by the advective processes. The spectral fixer is the amount added to fill the negatives, which is balanced by a decrease elsewhere to ensure conservation.

In January, the fixer in the semi-Lagrangian case is about 3% of the total precipitation, while in the spectral case it is close to 10%. They are smaller in July, but the ratio of the 2 methods remains 3 to 1. These values are about 20 and 60% of those found with CCM1 (Rasch and Williamson, 1990b). The semi-Lagrangian value is comparable to, or perhaps slightly smaller than that for the NMC model, while the spectral value is somewhat larger (Williamson, 1990). Some of the difference in conservation characteristics between CCM1 and CCM2 might be due to different characteristics in the scales of forcing by the parameterizations. However, much of the improvement over CCM1 is more likely attributable to the additional vertical resolution in CCM2, which is comparable to the resolution used in the NMC experiments. Rasch and Williamson (1990b) showed that much of the lack of conservation in the semi-Lagrangian version of CCM1 was associated with the vertical approximations, but only about half of the negative values in the spectral version were from the vertical aspects. This would also explain why the spectral case shows less improvement with higher vertical resolution, since a large fraction of the negative values are caused by the horizontal spectral truncation. Some of the lack of conservation in the semi-Lagrangian version may also be attributable to inconsistancies between the vertical advection of the water vapor mixing ratio and the corresponding vertical advection of mass of the air itself. This is not an issue with the spectral version, as the vertical finite difference approximations for moisture advection there are designed to be consistent with the transport of mass. Thus, in the absence of other issues (such as horizontal transport of the log of surface pressure), the spectral model algorithm will conserve moisture exactly. Rasch and Williamson (1991) show that the vertical advection scheme, which is applied to the mass of the atmosphere (finite difference), had different characteristics than those applied to the specific humidity (semi-Lagrangian), with the 12 levels of CCM1. We will see later that, with the 18 levels of CCM2, the characteristics of the 2 forms of advection are not as different, although they are still not identical. In contrast to the vertical advection, the characteristics of the horizontal semi-Lagrangian and spectral advections are similar in the lower troposphere away from the polar regions, where most of the mass of the water vapor is found. Thus, inconsistencies in the horizontal advection of atmospheric mass (spectral) and water vapor specific humidity (semi-Lagrangian) are less likely to be responsible for non-conservation. The conclusion that much of the lack of conservation is due to the vertical aspects is also supported by the observation that the conservation is only marginally affected by the horizontal resolution. The corresponding values of the conservation fixer from January simulations with a preliminary version of CCM2 with 18 levels at T31, T42 and T63 resolutions are $-0.12$, $-0.11$, and $-0.10$ mm/day, respectively.

The difference between the spectral and semi-Lagrangian case is larger for the stable precipitation than for the convective precipitation, even though the convective precipitation is over three times larger. The increased stable precipitation is associated with the spectral negative filler. We propose the following mechanism for the increase in stable precipitation: (1) the negative values in a region are filled to zero, which can result in an increase in the local (horizontal) area average; (2) the spectral advection (truncation) then re-introduces oscillations with positive values overshooting local saturation, and zero values again becoming negative; (3) the supersaturated areas are then returned to saturation through stable condensation. The process is then repeated. This mechanism provides a path for computational transport into regions of small water vapor and then condensation.

The total precipitable water is 0.3 to 0.5 mm larger in the semi-Lagrangian simulation than in the spectral. This is comparable in magnitude to the difference found in CCM1, but of opposite sign. The semi-Lagrangian values in CCM2 are close to the observed estimates of 24.6 and 28.6 mm for January and July, respectively (Peixoto and Oort, 1983; Trenberth et al., 1987).

## 5. January zonal averages

We now consider the zonal averages from the 2 simulations and their differences. Differences

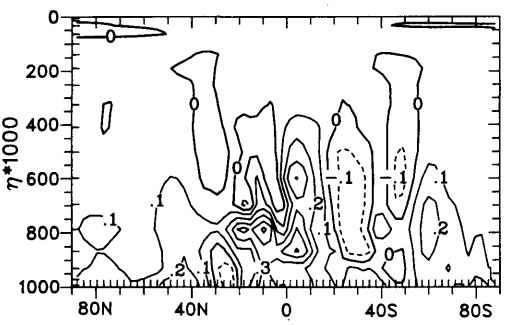


*Fig. 1.* January average, zonal average difference of specific humidity for semi-Lagrangian minus spectral. Contour interval is 1.0 g/kg.

always represent the semi-Lagrangian minus the spectral.

Fig. 1 shows the January mean of the zonal average difference in specific humidity. The zonal average specific humidity from CCM2 is shown in Hack (1993). The semi-Lagrangian case has higher specific humidity in the troposphere in both polar regions, in the ascending branch of the Hadley cell, and in the descending branch in the northern hemisphere near the trade inversion. The semi-Lagrangian case has lower values in the descending branch in the southern hemisphere. The net difference suggests the semi-Lagrangian simulation is moister, as seen earlier in the global average precipitable water. The difference in precipitable water is probably significant, as the value from the spectral simulation is smaller by 0.1 mm than the smallest value of the 20 individual Januaries of the semi-Lagrangian control and differs from the mean by 2.5 × the standard deviation of the 20 values from the control which is a little less than 0.2 mm. The differences in the zonal average specific humidity in Fig. 1, however, would not be accepted as significant in a pointwise test. The pointwise differences between individual years of the control, and the 20 year average are as large as those in Fig. 1. However, the pattern of the difference in Fig. 1 is characteristically different from those of individual years. The individual differences are more vertically oriented with narrower regions of positive and negative values associated with the interannual variability in the migration of the ITCZ. Fig. 1 shows a much broader region of positive differences northward of −20° latitude. Some examples of differences for individual years of the control will be discussed in Section 7.

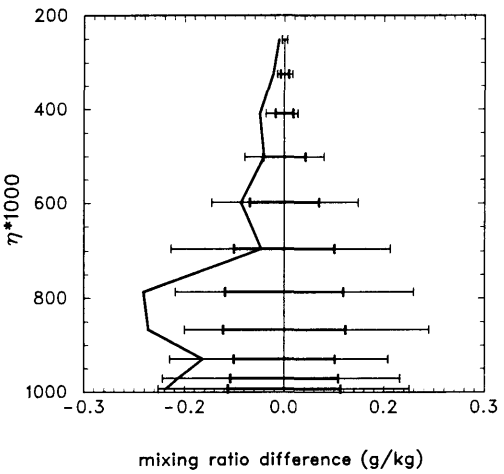


*Fig. 2.* Standard deviation (thick bars) and minimum and maximum (thin bars) of the difference of the 20 individual Januaries from the 20-year January average of the control semi-Lagrangian simulation and difference of the January average of the spectral simulation from the 20-year average of the control for the zonal average specific humidity averaged from −30 to +30 latitude.

Thus, although the pointwise differences cannot be shown to be significant, the pattern probably is. Fig. 2 quantifies this difference further. It shows the difference of the January average of the spectral simulation from the average of the 20 Januaries of the control for the zonal average mixing ratio averaged from −30 to +30 latitude. In addition, the standard deviation of the differences of the individual Januaries from the 20 year average of the control is shown by the thick bars, and the minimum and maximum differences by the thin

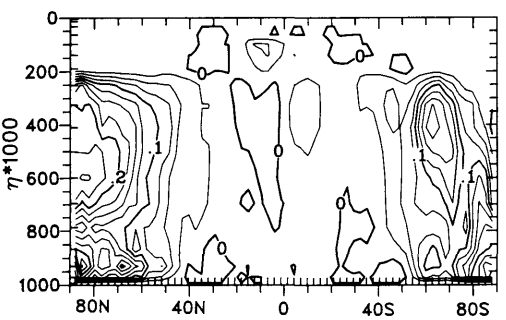


*Fig. 3.* January average, zonal average difference of cloud fraction for semi-Lagrangian minus spectral. Contour interval is 0.025.

bars. If we assume the population distribution is normal, with a standard deviation of the 20-member sample, the specific humidity of the spectral simulation at 800 mb and the level below would be significantly different from that of the semi-Lagrangian at the 5% level, since the differences exceed 2 standard deviations. Whether or not the simulations are actually significantly different, the important point that will be shown in the following discussion, is that the two simulations result from very different balances of processes.

In CCM2, the mid latitude and polar differences are larger than in CCM1. The tropical and extratropical differences were horizontally layered in the troposphere in CCM1, but are vertically oriented corresponding to the Hadley circulation in CCM2. The semi-Lagrangian case is moister in CCM2 above 500 mb, while it was drier in CCM1. The different signature is presumably due to the fundamental differences in the physical parameterizations in the two models, most notably the PBL and convective parameterizations coupled with the changed vertical resolution.

The January global average cloudiness drops from 0.55 with semi-Lagrangian advection to 0.47 with spectral advection in CCM2, whereas with CCM1 the relative change was slightly larger, going from 0.50 to 0.40. The difference in the CCM2 values is clearly significant, as the minimum value for the 20 years of the semi-Lagrangian control is 0.54, and the standard deviation is less than 0.003. The zonal average difference is shown in Fig. 3. The zonal average cloud fraction is shown in Hack (1993). The differences occur poleward of 40° and below the tropical tropopause. The differences poleward of 70° latitude would not pass a pointwise significance test, a the variability from year-to-year in the semi-Lagrangian control is as large. However, the differences of individual years do not have a uniform sign over regions of such large extent. Selected differences for individual years of the control will be discussed later in Section 7. Again, the pattern implies that the differences in Fig. 3 are significant. The greenhouse effect of the high clouds can be seen in the outgoing longwave radiation and temperature fields, which will be discussed later. The tropical high cloud differences in CCM2 forming north of the ascending branch of the Hadley cell were not apparent in CCM1. Poleward of 40°, the changes in CCM2 are the same sign as but larger than those in CCM1. The low cloud differences in CCM1 (associated with the layered moisture difference in CCM1) are not present in CCM2.

The difference in the longwave radiative heating (semi-Lagrangian minus spectral) is shown in Fig. 4. To a large extent, the differences in polar regions and mid troposphere tropics are responses to changes in the cloud field with relative warming below the increased clouds and relative cooling in and above the increased clouds. This signature in the radiation difference is very different from that in CCM1, where all terms were consistent with the layered lower troposphere differences associated with the low cloud differences.

Except in the dark northern hemisphere, the difference in the shortwave heating (Fig. 5) is of opposite sign to (but smaller in magnitude by about 25% than) the longwave radiative heating difference. This difference partially compensates

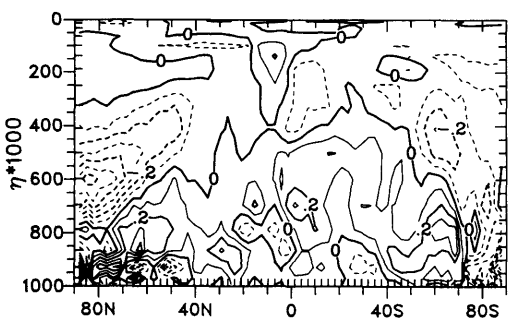


*Fig. 4.* January average, zonal average difference of longwave radiative heating for semi-Lagrangian minus spectral. Contour interval is 0.10 K/day.

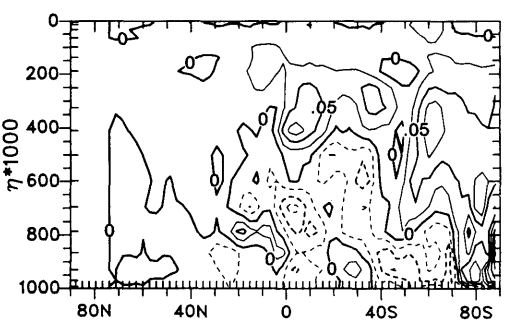


*Fig. 5.* January average, zonal average difference of solar radiative heating for semi-Lagrangian minus spectral. Contour interval is 0.025 K/day.

the longwave difference and changes the balance by that amount. This compensation could have important implications for sensitivity studies of processes affecting only 1 of the 2 terms. The 2 model versions would indicate different sensitivities. (*Note*, this sensitivity does not suggest that both models are equally bad, but rather that another criterion is needed to judge suitability or unsuitability of the models, e.g., whether one model is physically more reliable. In the case of these 2 models, we will show later that the spectral version has undesirable properties, namely that the negative fixer is a dominant process in the regions where the clouds are different and therefore where the radiation is different.)

The vertical moisture advection is somewhat more vigorous in CCM2 (Fig. 6, bottom) than in CCM1 (Fig. 11 of Rasch and Williamson, 1991). The relative drying in the northern hemisphere subsidence region is 50 % stronger and has a higher vertical extent. The moistening in the upward branch is distributed throughout the column, rather than being concentrated in the lower troposphere. The local maximum is not as large as in CCM1, but occurs higher in the troposphere. In addition, the upward branch produces drying in the lower troposphere, as the Hadley cell is more effective in transporting moisture upward out of the PBL. Overall, in CCM2 the semi-Lagrangian version is more active than the spectral version in the upward and downward branches of the Hadley cell. The difference is shown in the top panel of Fig. 6. The moistening in the upward branch in the semi-Lagrangian is double that in the spectral. The drying in the descending branch extends higher in the semi-Lagrangian.

The differences between the vertical advection in the two simulations may be due to the numerical formulation itself, or may be due to the differences in the water vapor distribution between the two simulations. The structure of the difference in vertical advection in CCM1 was directly attributable to the different numerical approximations. This is also the case in CCM2 below 700 mb. The difference there looks like the difference (not shown) seen when the vertical advection operator of the spectral model (recall, this is actually a finite difference operator) is applied to the water vapor simulated by the semi-Lagrangian version. For example, the finite difference advection does not maintain as thin a region of drying at the base of the upward branch of the Hadley cell. Above 700 mb, however, the differences in CCM2 are not simply attributable to the numerical approximations. Other processes are contributing to the differences there. The signature of the difference in CCM2 is different than that in CCM1. In CCM1 the vertical advection tended to moisten the semi-Lagrangian simulation relative to the spectral around 800 mb and dry above and below. Fig. 6 shows that, in CCM2, the semi-Lagrangian vertical advection, relative to the spectral, tends to moisten the atmosphere throughout the entire column, almost to the tropopause.

In the tropics, the difference in horizontal moisture advection (Fig. 7) partially compensates the difference in the vertical advection, although the horizontal difference is considerably noisier. This compensation is perfectly natural, as the two advection terms are intimately connected through the motions comprising the Hadley cell structure of the atmosphere. The difference in CCM2 is smaller than in CCM1. In CCM2, part of the dif-

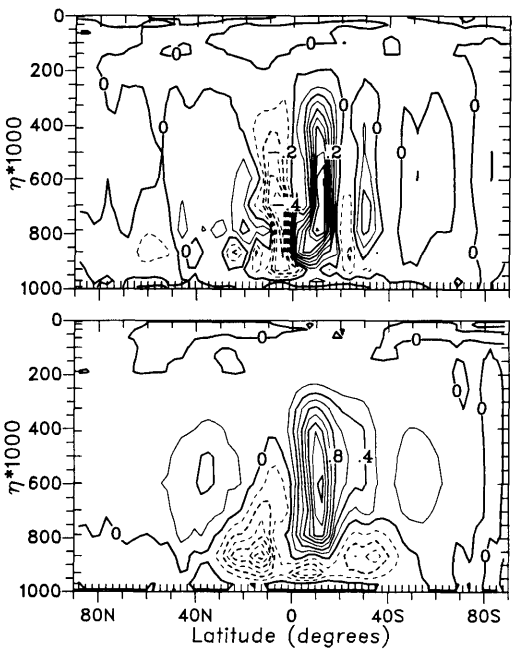


*Fig. 6.* January average, zonal average vertical moisture advection for semi-Lagrangian simulation (bottom) and the difference, semi-Lagrangian minus spectral (top). Contour interval is 0.2 g/kg/day for the field and 0.1 g/kg/day for the difference.

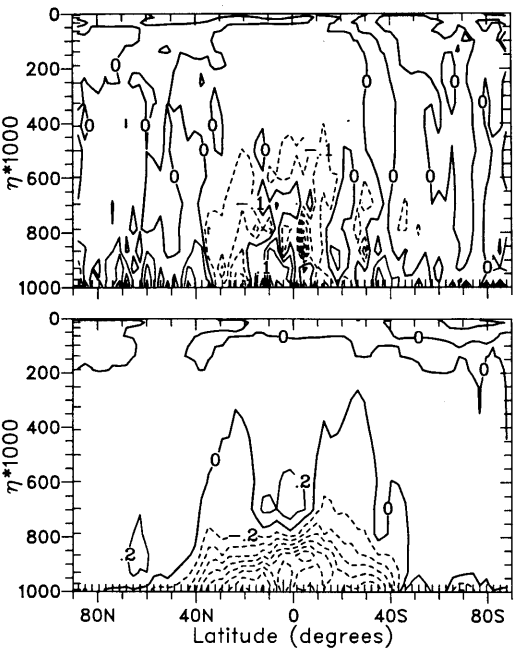


*Fig. 7.* January average, zonal average horizontal moisture advection for semi-Lagrangian simulation (bottom) and the difference, semi-Lagrangian minus spectral (top). Contour interval is 0.2 g/kg/day for the field and 0.1 g/kg/day for the difference.

ference is due to the different advection operators. The contribution of the advection operators to the difference was less noticeable in CCM1, where the states themselves were more different and dominated the horizontal advection difference.

The difference in the specific humidity tendency, from the vertical diffusion (Fig. 8), which includes the PBL parameterization, is small in much of the domain. The semi-Lagrangian version has less moistening at the top of the PBL in the tropics than the spectral. There is also less moistening in northern mid-latitudes near the surface. A direct connection can be seen between the vertical diffusion differences and condensation (stable and convective) differences examined below.

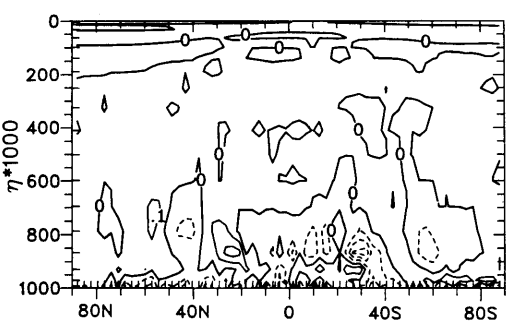


*Fig. 8.* January average, zonal average difference of specific humidity tendency from the vertical diffusion for semi-Lagrangian minus spectral. Contour interval is 0.1 g/kg/day.

The difference in the specific humidity tendency, due to condensation and convective transport (Fig. 9, top), partially compensates the vertical advection difference in the mid and upper tropical troposphere. The condensation is from both stable and convective parameterizations. The semi-Lagrangian has larger condensation, leading to stronger condensational heating. This in turn forces stronger vertical motion, yielding larger vertical advection. Of course, cause and effect cannot be sorted out in this circular chain. Note, the convective parameterization includes a mass transport and hence the positive tendencies from detrainment in the subsidence regions (Fig. 9, bottom).

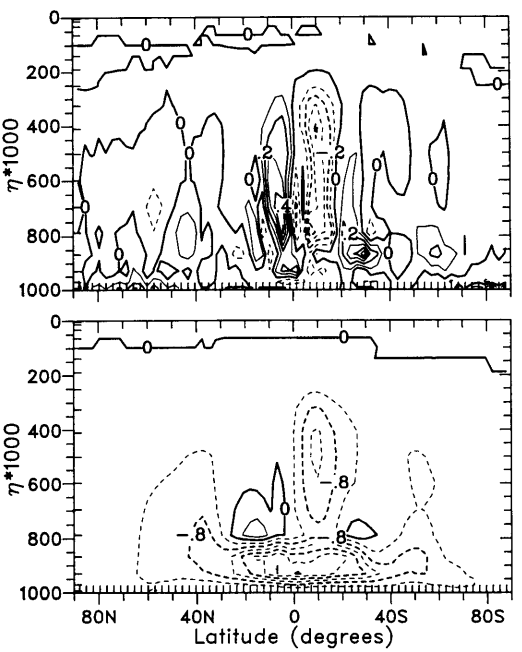


*Fig. 9.* January average, zonal average specific humidity tendency due to condensation and convective transport for semi-Lagrangian simulation (bottom) and the difference, semi-Lagrangian minus spectral (top). Contour interval is 0.4 g/kg/day for the field and 0.1 g/kg/day for the difference.

Fig. 10 shows the inverse time scale of vertical moisture advection for semi-Lagrangian and spectral simulations. The inverse time scale of a term in the moisture budget is calculated as the zonal average of the term itself, divided by the zonal average of the mixing ratio. The larger the inverse time scale, the smaller the time scale itself, and the faster the process acts to modify the specific humidity. Thus the term "faster" implies the process is more important in determining the moisture budget in a given region and "slower" implies it is less important. The semi-Lagrangian vertical advection is somewhat faster, however CCM2 does not show the relatively large difference in upper tropical troposphere seen in CCM1. The difference in CCM1 was attributable to the different advection approximations, rather than to a different simulated state. The small sensitivity in CCM2 implies the additional vertical resolution in CCM2 has resulted in the two vertical advection schemes being closer to each other. This observation is also consistent with the improved moisture conservation in CCM2, although the moisture in the levels being emphasized in the vertical advection inverse time scale makes a relatively small contribution to the global average mass of moisture.

Fig. 11 shows the inverse time scale of horizontal moisture advection for the semi-Lagrangian and spectral simulations. The spectral version is significantly faster in the upper tropical troposphere. It should be kept in mind, however, that the horizontal advection is a small part of the budget there, as it is slow compared to vertical advection (its inverse time scale being 10% that of the vertical.) The horizontal advection is a very active process in the spectral simulation in the polar troposphere, especially in the winter hemisphere. Implicitly, the horizontal advection includes the truncation inherent in the spectral method. Its effect is clearly seen as a very fast process with latitudinal grid scale structure in the horizontal advection. This structure is completely consistent with that seen in the spectral CCM1.

Some term must balance the horizontal advection in the polar regions. Fig. 12 indicates it is the

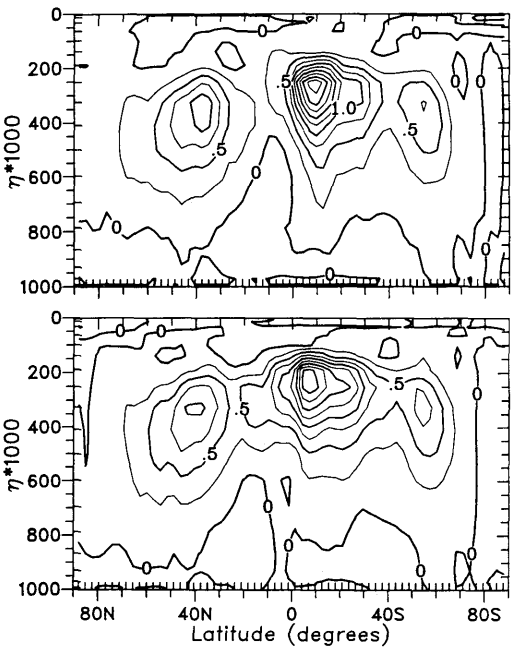


*Fig. 10.* January average, zonal average inverse time scale of vertical moisture advection for semi-Lagrangian (top) and spectral (bottom) simulations. Contour interval is 0.25 day$^{-1}$.

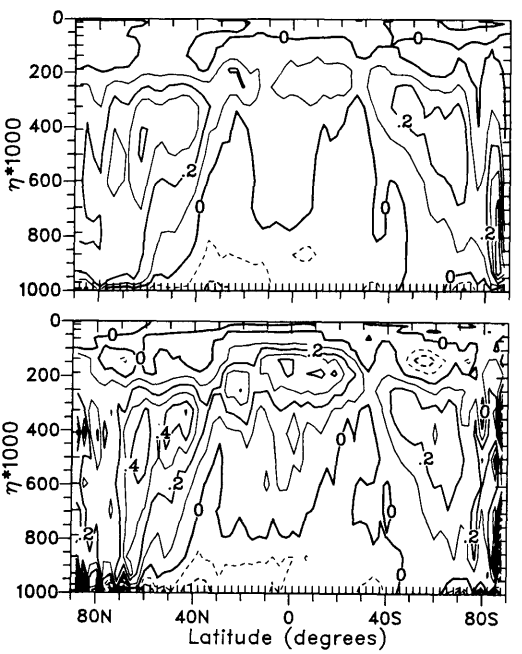


*Fig. 11.* January average, zonal average inverse time scale of horizontal moisture advection for semi-Lagrangian (top) and spectral (bottom) simulations. Contour interval is 0.1 day$^{-1}$.

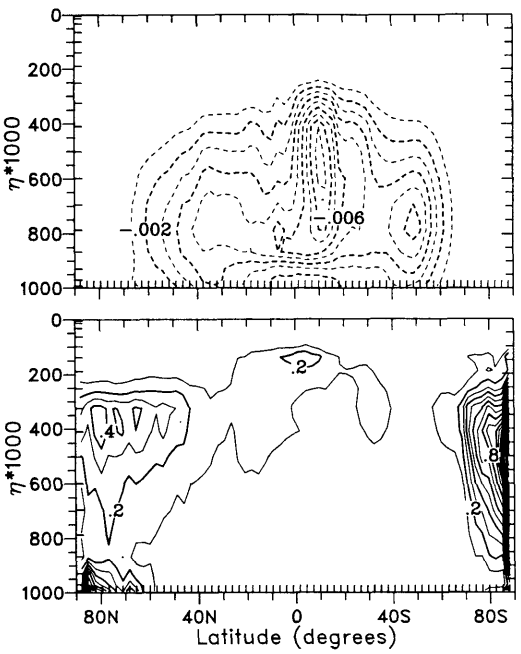


*Fig. 12.* January average, zonal average inverse time scale of conservation fixer for the semi-Lagrangian simulation (top) and the negative filler for the spectral simulation (bottom). Contour interval is 0.001 day$^{-1}$ for the semi-Lagrangian and 0.1 day$^{-1}$ for the spectral.

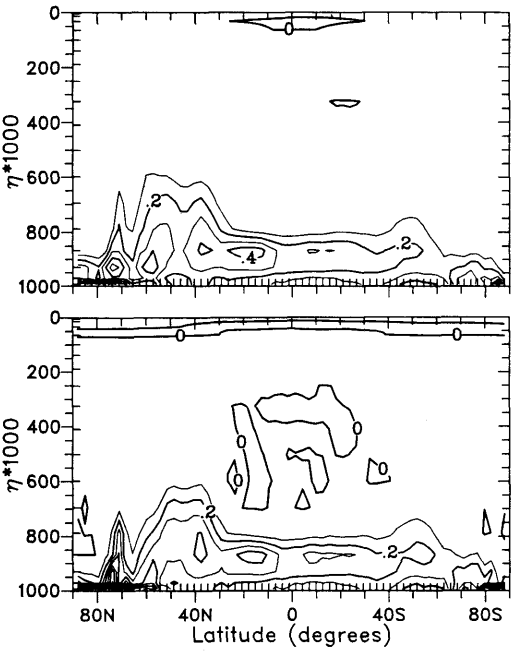


*Fig. 13.* January average, zonal average inverse time scale of vertical diffusion for semi-Lagrangian (top) and spectral (bottom) simulations. Contour interval is 0.1 day$^{-1}$.

spectral fixer used to keep the specific humidity non-negative. In the spectral version, this is a fast process in the troposphere in both polar regions. It is slower in CCM2 than in CCM1, by a factor of 10 near the tropical tropopause, perhaps because CCM2 is moister there. Nevertheless, it still represents an important process in the spectral form of CCM2 and contributes to condensation, as will be shown shortly. It also remains a dominant process in the winter polar surface region. Note that the conservation fixer included with the semi-Lagrangian scheme is 100 times slower than the negative filler of the spectral (the contour interval has been changed). It is distributed throughout the tropical and mid-latitude troposphere and resembles the specific humidity field itself, modulated by the total advection, consistent with its design.

The inverse time scale of the vertical diffusion is shown in Fig. 13 for the 2 simulations. They are fairly similar, except the spectral shows larger values poleward of 70N. The transport in the semi-Lagrangian simulation in the PBL also tends to be active there, but not to the extreme seen in the spectral version. The horizontal advection (Fig. 11) must be changing the state enough to kick off additional, spurious PBL mixing in this region. This PBL mixing is balanced by the horizontal advection and condensation, as seen in Fig. 14. The preceding discussion provides an example of another physical process being adversely affected by the spectral advection negative fixer.

Fig. 14 shows the inverse time scale of the combination of the stable condensation and convective parameterization. Condensation occurs in mid-tropospheric polar regions in the spectral simulation, as the result of a source attributable to the negative fixer (Fig. 12). The process is as follows: the filler moves moisture into the polar regions to fill negative regions, the spectral truncation then redistributes it, generating negatives (undershootings) again and overshootings, which can be supersaturated. Condensation then removes the

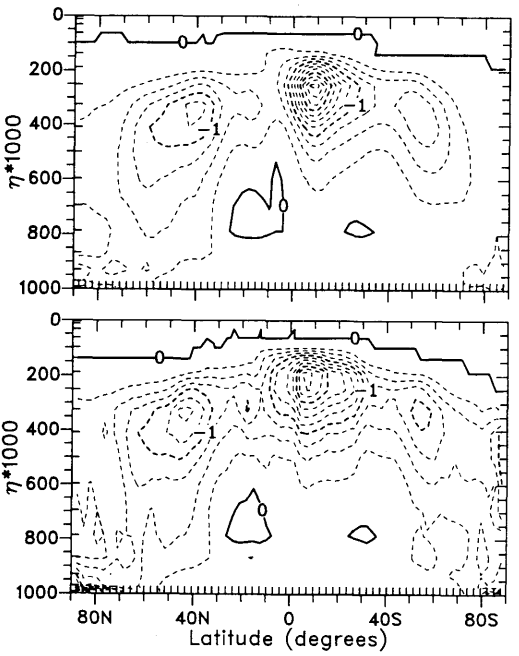


*Fig. 14.* January average, zonal average inverse time scale of water vapor tendency due to stable condensation and convective parameterization for semi-Lagrangian (top) and spectral (bottom) simulations. Contour interval is 0.25 day$^{-1}$.

supersaturation. Condensation is also slightly faster in the spectral simulation in the upper tropical troposphere, in partial response to the fixer (recall, however, that both vertical and horizontal advections are also faster there in the spectral and both act as sources there.) The tropical tropopause and upper troposphere mid-latitude storm track regions show smaller differences than in CCM1. This smaller sensitivity is consistent with the difference in the fixers as well. In CCM1 the fixer in these regions was probably partially driven by physics (the moist adiabatic adjustment in particular), which induced large horizontal gradients that the spectral advection could not handle, thus invoking the fixer and subsequently causing condensation. The physical parameterizations are more spatially coherent in CCM2. This observation follows from the examination of other fields that are not shown in this paper, but available in papers cited above.

Fig. 15 shows the difference in the zonal average temperature between the semi-Lagrangian and

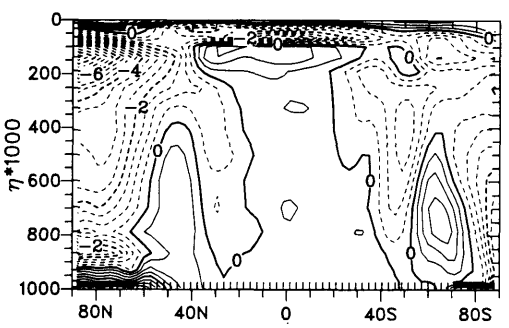


*Fig. 15.* January average, zonal average temperature difference, semi-Lagrangian minus spectral. Contour interval is 1.0 K.

spectral simulations. The temperature field from the semi-Lagrangian simulation is available in Hack (1993). Although the details of the moisture balance in the two simulations are very different, the temperature field shows only small differences throughout the tropical troposphere. Much of the extra-tropical difference is indistinguishable from the natural variability of the model. Potentially significant differences between the two models may exist in the stability characteristics of the lower polar troposphere, the warmer upper tropical troposphere, and the colder tropical stratosphere in the semi-Lagrangian simulation. The response in the temperature field in CCM2 to the moisture transport is very different than the response was in CCM1. In CCM1, except at the first model level near the North Pole, the entire troposphere was colder, with the differences exceeding 3 and 4° throughout much of the upper troposphere with semi-Lagrangian water vapor transport. The stratosphere in CCM1 was warmer by 3 to 4° with semi-Lagrangian water vapor transport. CCM2 shows the opposite signal near the tropical tropopause, warmer below and colder above, with the semi-Lagrangian transport.

## 6. July zonal averages

The general characteristics of the differences between the semi-Lagrangian and spectral simulation July zonal averages of the terms examined in the previous section are similar to those for January, if the winter hemisphere is compared to winter and the summer to summer. However, the resulting balance in July is somewhat different,

resulting in seasonal differences in the sensitivity of the temperature and moisture fields to the transport scheme. These differences are shown in Fig. 16 for specific humidity (top) and temperature (bottom).

The most notable differences between the July and January (Fig. 1) specific humidity differences occur in the summer extratropics. The midlatitude summer lower troposphere is drier in the semi-Lagrangian simulation in July, and the summer hemisphere polar region is moister. The polar differences are not significant, compared to the natural variability. There are several examples in the 20 years of the control where individual Julys show similar differences with the control. The mid latitude differences are likely to be significant. There are no examples in the control where the difference is of uniform sign over the entire region, as seen in Fig. 16. The July simulations show similar temperature differences to the January ones in the tropical troposphere, except the July differences in the upper troposphere are more confined to the equatorial region. The change in stability of the lower winter troposphere is not evident in the July simulation, nor is the change in the summer polar lowest level temperature. Most of the remaining July temperature differences are inseparable from the natural variability. Those which are not are the differences in the Northern Hemisphere upper troposphere and the large differences in the stratosphere.

## 7. Simulation without conservation correction

The correction applied to the moisture field to maintain conservation with the semi-Lagrangian transport scheme is ad hoc and justifiable only if it does not interact spuriously with the physical parameterizations. We have seen no indication that this is not the case. The correction could also be eliminated if the lack of conservation did not adversely affect the simulation. We have performed an additional simulation in which the conservation correction was not applied in a semi-Lagrangian simulation. This simulation also started on 1 September of the 11th year of the semi-Lagrangian control run. We present statistics from the following January.

Fig. 17 shows the difference in specific humidity for the semi-Lagrangian simulation without the conservation adjustment, minus that with the adjustment. The differences are within the natural variability of the control simulation, as seen by a comparison with Fig. 18. This figure shows the differences of four individual Januaries from the

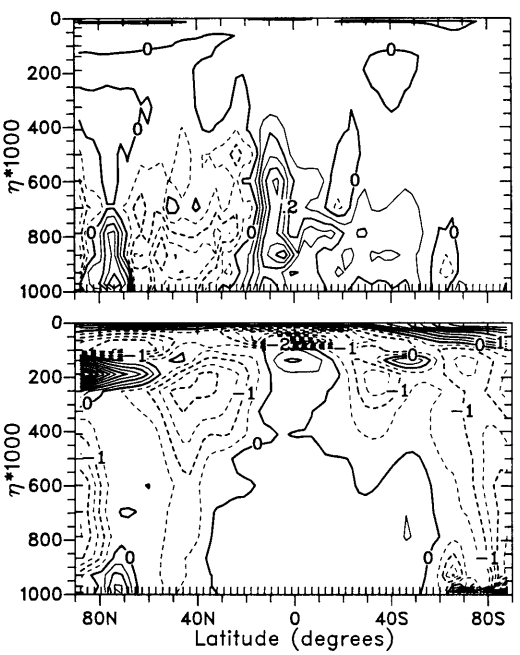


*Fig. 16.* July average, zonal average difference of specific humidity (top) and temperature (bottom), semi-Lagrangian minus spectral. Contour interval is 0.1 g/kg for specific humidity and 1.0 K for temperature.

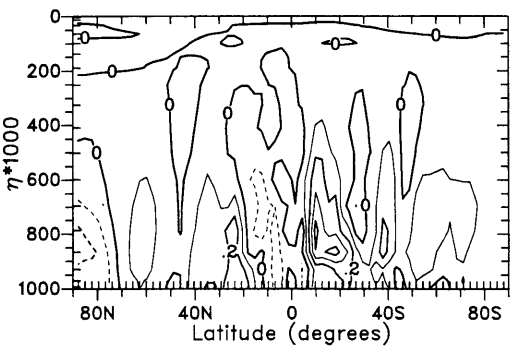


*Fig. 17.* January average, zonal average difference of specific humidity, semi-Lagrangian without conservation fixer minus semi-Lagrangian with. Contour interval is 0. 1 g/kg.

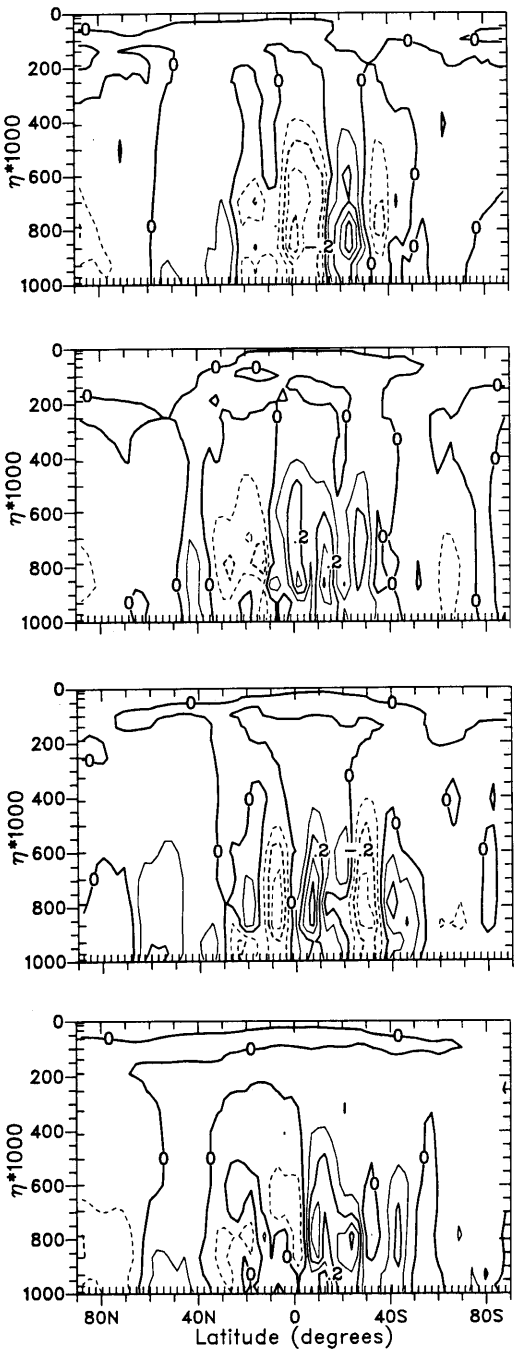


*Fig. 18.* January average, zonal average difference of specific humidity, four individual Januaries from the control minus the 20-year average. Contour interval is 0.1 g/kg.

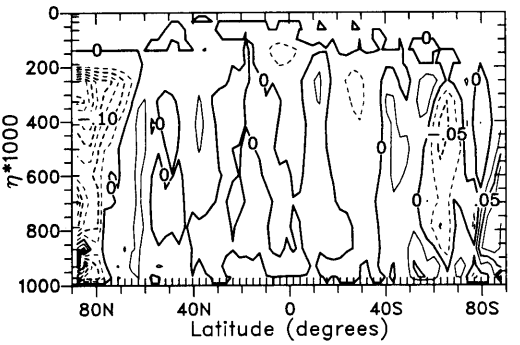


*Fig. 19.* January average, zonal average difference of cloud fraction, semi-Lagrangian without conservation fixer minus semi-Lagrangian with. Contour interval is 0.025.

control with the 20-year average. The particular examples were chosen to illustrate similarities with Fig. 17. As seen in these figures, there is no feature in the pattern or magnitude to distinguish Fig. 17 from the panels in Fig. 18.

All other terms examined also have differences which cannot be distinguished from the natural variability. As one other example, we present the zonal average cloud fraction difference in Fig. 19 and four samples of individual months from the control differenced with the 20 year average in Fig. 20. The cloud fraction is sensitive to most processes included in the model. Differences in any one would likely lead to differences in the cloud fraction. The difference in cloud fraction associated with including or excluding the fixer has no characteristics to distinguish it from the natural variability.

The semi-Lagrangian scheme results in a computational source of moisture that the conservation fixer removes. When the adjustment is not

Table 2. *Global average values of various quantities associated with water vapor from semi-lagrangian simulations with and without the conservation adjustment*

| | January | | | |
|---|---|---|---|---|
| | with adjustment | | | without |
| | min | ave | max | adjustment |
| convective precip (mm/day) | 2.59 | 2.63 | 2.69 | 2.71 |
| stable precip (mm/day) | 0.83 | 0.85 | 0.87 | 0.89 |
| total precip (mm/day) | 3.43 | 3.48 | 3.55 | 3.60 |
| evaporation (mm/day) | 3.42 | 3.49 | 3.55 | 3.51 |

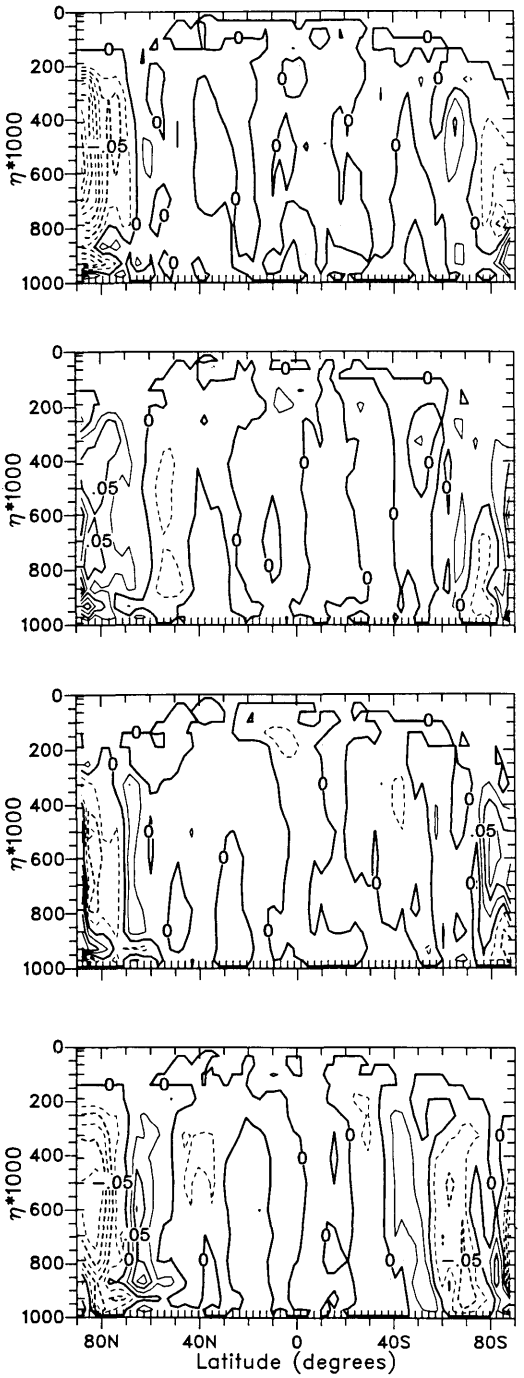


*Fig. 20.* January average, zonal average difference of cloud fraction, four individual Januaries from the control minus the 20-year average. Contour interval is 0.025.

applied, the moisture gain from the advection represents energy added to the system that did not arise from a physical source, but which can be released by condensation. The figures above show that the release of this spurious energy does not affect the simulation. It is small, compared to the energy associated with the physical mechanisms driving the system. The moisture source in the simulation without the conservation adjustment is given in Table 2, in terms of evaporation and precipitation. The values from the simulation with adjustment are repeated from Table 1, along with the minimum and maximum January averages from the 20 year simulation. In the case without adjustment, the difference between precipitation and evaporation (0.09) is close to the global average of the adjustment in the other case (0.10, Table 1). Without the adjustment, the precipitation is slightly larger than the maximum of the 20-year control simulation. The evaporation remains well within the natural variation of the control.

## 8. Conclusions

The balance of processes that produces the climate of CCM2 is very sensitive to the discrete water vapor transport algorithm, when comparing spectral with semi-Lagrangian. CCM2 is as sensitive as CCM1 was, however, the details of the sensitivity in CCM2 differ from those found earlier in CCM1. The observation that the balance is different when the water vapor transport algorithm is changed has important ramifications for climate sensitivity studies in which modified components affect one process more strongly than others. The 2 transport versions could indicate very different climate sensitivities in such cases. As mentioned earlier, such differences between two models do not indicate that both models are equally unsuitable for certain uses, but rather that other criteria are needed to judge their suitability. Such criteria could include whether one of the models has an identifiable computational shortcoming, or whether the components of one model are thought to be more physically reliable. The former criteria serves to eliminate a model without judging the other, which may have similarly serious, but still hidden, shortcomings. The second example gives preference to a model thought to be more physi-

cally reliable, based on consideration of its individual components. In the case at hand, the components are identical, except the numerical moisture transport. The spectral transport clearly has shortcomings. The negative fixer is a dominant process in the moisture forecast in significant regions of the domain. This leads to an incorrect balance in polar regions in particular, where the fixer dominates. This is also the region where the simulations show the largest difference. The semi-Lagrangian scheme does not have any identified shortcoming, other than the lack of conservation, that requires a fixer. Unlike the spectral simulation, however, this fixer seems to be cosmetic and has, as yet, no identified adverse effect on the simulation. In fact, elimination of the fixer results in a simulated climate that falls within the natural variability of the 20-year control simulation, both in terms of the state variables and the processes that balance to produce that state.

The simulations described here corroborate the conclusions of Rasch and Williamson (1991), which also pointed out that simulations based on CCM1, with the 2 different water vapor transport schemes, involve delicate balances between the various components of the atmospheric system. In the current study with CCM2, although we have changed the same component (the water vapor transport), the temperature and moisture responses have been quite different from those of the previous study. In fact, they are even of opposite sign in some fields. On the other hand, the direct influence on many of the processes, such as horizontal and vertical advection and condensation, has been the same. It is clear that even with the more realistic thermal and moisture structures being driven by the new physical parameterizations in CCM2, errors in the spectral transport can directly influence the model climate.

## 9. Acknowledgements

We would like to thank Jerry Olson for developing the semi-Lagrangian component of CCM2 and James Hack and Jeffrey Kiehl for very helpful comments on earlier versions of the manuscript. We would also like to thank the anonymous reviewers for their suggestions and Janet Rodina for editorial improvements.

## Appendix

*Water vapor prediction in CCM2*

The specific humidity ($q$) prediction equation is written

$$\frac{\partial q}{\partial t} = -V\cdot\nabla q - \dot{\eta}\frac{\partial q}{\partial \eta} + S + A + F, \tag{A1}$$

where $t$ is time; $V$ is the horizontal velocity; $\eta$ is the transformed vertical coordinate; $\dot{\eta}$ is the vertical velocity in that system; $S$ is the source/sink associated with physical parameterizations formulated as tendencies (surface flux and vertical diffusion); $A$ the effective source/sink associated with physical parameterizations formulated or applied as adjustments (convective parameterization, large scale stable precipitation and dry convective adjustment, which also mixes water vapor); and $F$ is the conservation adjustment term.

The basic time step proceeds as a series of time split substeps that can be thought of as sequentially approximating the individual equations

$$\frac{\partial q}{\partial t} = S, \tag{A2}$$

$$\frac{\partial q}{\partial t} = -V\cdot\nabla q - \dot{\eta}\frac{\partial q}{\partial \eta}, \tag{A3}$$

$$\frac{\partial q}{\partial t} = F, \tag{A4}$$

$$\frac{\partial q}{\partial t} = A, \tag{A5}$$

by the discrete forms:

$$q^{-} = q^{n-1} + 2\,\Delta t S, \tag{A6}$$

$$\hat{q}^{+} = L_{\lambda\phi\eta}(q^{-}), \tag{A7}$$

$$q^{+} = \hat{q}^{+} + 2\,\Delta t F, \tag{A8}$$

$$q^{n+1} = A(q^{+}). \tag{A9}$$

Step (A6), consisting of the surface flux, PBL parameterization, and vertical diffusion, is detailed in Holtslag and Boville (1993). In the semi-Lagrangian step (A7), $L_{\lambda\phi\eta}$ represents the interpolation operation applied at the departure point

and will be explained in more detail shortly. The conservation fixing step (A8) is of the form

$$F=\frac{\alpha}{2\,\Delta t}\,\hat{q}^{+}\,|\hat{q}^{+}-q^{-}|^{\beta}, \tag{A10}$$

where $\beta=\frac{3}{2}$ and $\alpha$ is determined for global conservation.

$$\int q^{+}\,\Delta p^{n+1}=\int q^{-}\,\Delta p^{n-1}, \tag{A11}$$

and the global integral is approximated by the normal Gaussian quadrature used in spectral models

$$\int q\,\Delta p=\sum_{i=1}^{I}\sum_{j=1}^{J}\sum_{k=1}^{K} q_{ijk}\,\Delta p_{ijk}\,w_j,$$

where the longitude index is $i$, latitude is $j$, and vertical is $k$. The Gaussian weights are $w_j$. Note the surface pressure and, thus, $\Delta p$ is unaffected by steps (A2), (A4), and (A5) hence, the eq. (A11) involves $\Delta p^{n+1}$ and $\Delta p^{n-1}$, rather than a $\Delta p^{+}$ and $\Delta p^{-}$. The coefficient $\alpha$ is given by

$$\alpha=\frac{\int q^{-}\,\Delta p^{n-1}-\int \hat{q}^{+}\,\Delta p^{n+1}}{\int \hat{q}^{+}\,|\hat{q}^{+}-q^{-}|^{\beta}\,\Delta p^{n+1}}. \tag{A12}$$

The adjustment physics of step (A9) includes the cumulus parameterization described by Hack (1993) and the large scale stable condensation and dry convective adjustment (applied to the top 3 model levels only) described by Williamson, et al. (1987). The equivalent tendency is obtained by

$$A=\frac{q^{n+1}-q^{+}}{2\,\Delta t}. \tag{A13}$$

The semi-Lagrangian advection step (A7) is further subdivided into horizontal and vertical advection sub-steps associated with

$$\frac{\partial q}{\partial t}+V\cdot\nabla q=0, \tag{A14}$$

$$\frac{\partial q}{\partial t}+\dot{\eta}\,\frac{\partial q}{\partial \eta}=0, \tag{A15}$$

as

$$q^{\circ}=L_{\lambda\phi}(q^{-}), \tag{A16}$$

$$\hat{q}^{+}=L_{\eta}(q^{\circ}). \tag{A17}$$

The horizontal trajectories associated with (A16) are calculated following Williamson and Rasch (1989), using the mixed spherical-geodesic scheme poleward of 70° and the global spherical scheme equatorward of 70° with central wind components at time $n$. One iteration is performed with the first guess of the midpoint being the trajectory midpoint from the previous time step. The vertical trajectory is calculated with the same algorithm applied in one dimension only.

The horizontal interpolation associated with $L_{\lambda\phi}$ of (A16) uses the tensor product Hermite cubic, with cubic derivative estimates modified to satisfy the $C^0$ sufficient condition for monotonicity (Williamson and Rasch, 1989). The vertical interpolation associated with $L_{\eta}$ of (A17) is also Hermite cubic with a zero derivative estimate at the top and bottom moisture levels. The moisture is assumed to be independent of $\eta$ outside these bounds and equal to the top or bottom grid value, as appropriate. The cubic derivative estimate is used at interior points. For the first point in from the boundaries, the derivative estimate calculated for the second interval is also used for the first interval. As with the horizontal estimates, the vertical derivative estimates are modified to satisfy the $C^0$ sufficient condition for monotonicity.

The timesplit decomposition of the advection into horizontal and vertical substeps reduces the formal truncation error from second order to first. This could lead to additional computational error with long time steps. However, we observe that this is not the case in our application. We have performed experiments with a non time split, three-dimensional version, and find no significant differences in the simulation compared to those for the time split version described here. The time step is constrained to be 20 min for the T42, 18 level version by the spectral dynamics. Occasionally, (in the southern hemisphere winter) winds in the top model level exceed a Courant number of one. When this occurs, dynamical variables at the top model level (only) are truncated below T42 to achieve a maximum Courant number of 1. We have not observed the vertical Courant number to exceed one in our simulations.

The semi-Lagrangian method contains some implicit damping associated with the interpolation. We exclude the explicit horizontal diffusion of specific humidity, which is included in the spectral version, to partially compensate for this. Although

we cannot isolate the damping introduced by the semi-Lagrangian, we find nothing that would indicate it is significant at the resolution adopted by CCM2. We also note that the semi-Lagrangian retains the smallest scales resolvable by the Gaussian grid, but removed by the spectral method. This additional resolution may contribute to the above observation concerning the damping.

## REFERENCES


Boville, B. A., Holton, J. R. and Mote, P. 1991. Simulation of the Pinatubo aerosol cloud in a general circulation model. *Geophys. Res. Lett.* **18**, 2281–2284.

Briegleb, B. P. 1992. Delta-Eddington approximation for solar radiation in the NCAR Community Climate Model. *J. Geophys. Res.* **97**, 7603–7612.

Hack, J. J. 1993. Parameterization of moist convection in the NCAR Community Climate Model, CCM2. *J. Geophys. Res.*, in press.

Hack, J. J., Boville, B. A., Briegleb, B. P., Kiehl, J. T., Rasch, P. J. and Williamson, D. L. 1993. *Description of the NCAR Community Climate Model (CCM2).* NCAR Tech. Note, NCAR/TN-382 + STR, 108 pp.

Holtslag, A. A. M., de Bruijn, E. I. F. and Pan, H.-L. 1990. A high resolution air mass transformation model for short-range weather forecasting. *Mon. Wea. Rev.* **118**, 1561–1575.

Holtslag, A. A. M. and Boville, B. A. 1993. Local versus nonlocal boundary-layer diffusion in a global climate model. *J. Climate.*, 1825–1842.

Kiehl, J. T. and Briegleb, B. P. 1991. A new parameterization of the absorptance due to the 15 $\mu$m band system of carbon dioxide. *J. Geophys. Res.* **96**, 9013–9019.

Laprise, R. 1988. Representation of water vapour in a spectral GCM. In: *Research activities in atmospheric and oceanic modelling.* G. J. Boer (ed.), CAS/JSC Working Group on Numerical Experimentation, Rep. No. 11, 3.18–3.21.

McFarlane, N. A. 1987. The effect of orographically excited wave drag on the general circulation of the lower stratosphere and troposphere. *J. Atmos. Sci.* **44**, 1775–1800.

Ostiguy, L. and Laprise, J. P. R. 1990. On the positivity of mass in commonly used numerical transport schemes. *Atmos. Ocean* **28**, 147–161.

Peixoto, J. P. and Oort, A. H. 1983. The atmospheric branch of the hydrological cycle and climate. In: *Variations in the global water budget*, pp. 5–65. D. Reidel, Norwell, Massachusetts.

Rasch, P. J. and Williamson, D. L. 1990a. On shape-preserving interpolation and semi-Lagrangian transport. *SIAM J. Sci. Stat. Comput.* **11**, 656–687.

Rasch, P. J. and Williamson, D. L. 1990b. Computational aspects of moisture transport in global models of the atmosphere. *Quart. J. Roy. Meteor. Soc.* **116**, 1071–1090.

Rasch, P. J. and Williamson, D. L. 1991. The sensitivity of a general circulation model climate to the moisture transport formulation. *J. Geophys. Res.* **96**, 13,123–13,137.

Rood, R. B. 1987. Numerical advection algorithms and their role in atmospheric transport and chemistry models. *Rev. Geophys.* **25**, 71–100.

Shea, D. J., Trenberth, K. E. and Reynolds, R. W. 1990. A global monthly sea surface temperature climatology. NCAR Technical Note, NCAR/TN-345 + STR, Boulder, CO, 167 pp.

Simmons, A. J. and Burridge, D. M. 1981. An energy and angular momentum conserving vertical finite-difference scheme and hybrid vertical coordinates. *Mon. Wea. Rev.* **109**, 758–766.

Simmons, A. J. and Strüfing, R. 1981. An energy and angular-momentum conserving finite-difference scheme, hybrid coordinates and medium-range weather prediction. ECMWF Technical Report No. 28, 68 pp.

Simmons, A. J. and Strüfing, R. 1983. Numerical forecasts of stratospheric warming events using a model with a hybrid vertical coordinate. *Quart. J. Roy. Meteor. Soc.* **109**, 81–111.

Slingo, J. M. 1987. The development and verification of a cloud prediction scheme for the ECMWF model. *Quart. J. Roy. Meteor. Soc.* **113**, 899–927.

Trenberth, K. E., Christy, J. R. and Olson, J. G. 1987. Global atmospheric mass, surface pressure and water vapor variations. *J. Geophys. Res.* **92**, 14815–14826.

Troen, I. and Mahrt, L. 1986. A simple model of the atmospheric boundary layer; Sensitivity to surface evaporation. *Boundary-Layer Meteor.* **37**, 129–148.

Williamson, D. L., Kiehl, J. T., Ramanathan, V., Dickinson, R. E. and Hack, J. J. 1987. *Description of NCAR Community Climate Model (CCM1).* NCAR Tech. Note, NCAR/TN-285 + STR, NTIS PB87-203782/AS, National Center for Atmospheric Research, Boulder, Colorado, 112 pp.

Williamson, D. L. and Rasch, P. J. 1989. Two-dimensional semi-Lagrangian transport with shape preserving interpolation. *Mon. Wea. Rev.* **117**, 102–129.

Williamson, D. L. 1990. Semi-Lagrangian moisture transport in the NMC spectral model. *Tellus* **42A**, 413–428.

Williamson, D. L. 1992. Review of numerical approaches for modeling global transport. *Air pollution modelling and its application IX*, ed., H. van Dop and G. Kallos. Plenum Press, NY, 377–394.